Full-Duplex mmWave Communication with Partially-Connected Hybrid Beamforming

Andrea Guamo-Morocho, Roberto López-Valcarce
atlanTTic Research Center, Universidade de Vigo, Vigo, Spain
Email: {aguamo,valcarce}@gts.uvigo.es

***Abstract*—Despite the potential of beamforming approaches to mitigate self-interference (SI) in multiantenna mmWave full-duplex (FD) systems, limitations imposed by practical hybrid beamforming architectures make the problem quite challenging. We present a novel design for the partially-connected array structure with finite-precision phase shifters, based on maximizing the product of the signal-to-SI-plus-noise ratios (SSINR) at receivers. Analog precoders and combiners are designed first under this criterion, with SSINR measured at the analog combiners' output. Using the effective channels for the analog beamformers so obtained, the baseband beamformers are then found using the same criterion, but with SSINR measured at the digital combiners' output. Simulations show that the proposed scheme outperforms existing FD approaches in terms of spectral efficiency and residual SI, even with low-resolution phase shifters.**

***Index Terms*—Partially-connected; Full-Duplex; mmWave; Hybrid Beamforming; Self-Interference Cancellation.**

I. Introduction

Confronting the unprecedented increase in the demand for data and services, next generation wireless communication systems will introduce new capabilities to boost performance and enable or expand new use cases [1]. Millimeter-wave (mmWave) communication, multi-input multi-output (MIMO) and in-band full-duplex (FD) operation have emerged as promising solutions to efficiently utilize available spectral, hardware, and energy resources [2]. Although mmWave signal propagation suffers from severe path loss, shadowing, and diffraction, these adverse effects can be mitigated by employing large antenna arrays and advanced beamforming techniques. However, conventional digital beamforming approaches are not practical as they require a dedicated radio frequency (RF) chain per antenna. The hybrid beamforming (HB) architecture is seen as a viable alternative with a reduced number of RF chains, thus offering a trade-off between flexibility and power consumption [3]. Two HB architectures are possible [4]: In the fully connected (FC) structure, all the antennas can connect to each RF chain, whereas in the partially connected (PC) structure the array is divided into subarrays, each of which connects to its own individual transceiver. Such array partitioning greatly reduces hardware complexity, although at the price of less overall array flexibility.

Through simultaneous data transmission and reception in the same frequency band, FD has the potential to double spectral efficiency (SE) with respect to half-duplex (HD) operation. Nevertheless, FD operation triggers self-interference (SI) at the receiver of the same transceiver, and to overcome this issue, SI cancellation (SIC) techniques become essential. These can be categorized into three levels [5], [6]. Whereas propagation domain SIC involves antenna subsystem design to minimize coupling, analog domain techniques attempt to substract an accurate copy of the SI signal from the received signal prior to analog-to-digital conversion (ADC), after which any residual SI should be cancelled in the digital domain. Analog domain SIC does not scale well with the number of antennas, and may be infeasible for large arrays; thus, it must be complemented with new beamforming techniques accounting for SI [7]. Of particular interest is the design of SI-aware beamformers for FD operation with hybrid architectures, as in [8]–[11], which focus on the fully connected (FD-FC) hybrid structure implemented with NL analog phase shifters, where N is the number of antennas and L is the number of RF chains. As mentioned above, the partially connected structure is preferable in terms of cost and consumption, since it only requires N phase shifters; however, given its more limited flexibility, it is unclear whether a full-duplex partially connected (FD-PC) hybrid architecture would still be effective to reduce SI, particularly when implemented with practical phase shifters enjoying limited phase resolution.

To the best of our knowledge, the only work on FD-PC is [12], whose design involves three steps. First, the optimal beamformers assuming all-digital arrays and no SI are obtained in terms of the dominant singular vectors of the corresponding channels. Then, these beamformers are projected onto the manifold defined by the partially connected structure using the SDR-AltMin algorithm from [13]. Finally, the digital precoders are replaced by the least dominant singular vectors of the effective SI channel. We provide an alternative FD-PC design that explicitly takes into account the limited resolution of phase shifters, improving on the method from [12] in terms of spectral efficiency. In addition, whereas [12] focuses on SI mitigation after digital combining, our approach targets SI reduction after analog combining. This is important in order to prevent loss of dynamic range in the ADC stage, as SI levels can be tens of dB above those of intended signals.

II. System Model

We consider a three-node mmWave system, where the transceiver at FD node $(\boldsymbol{a})$ (*e.g.,* a base station) simultaneously transmits to node $(\boldsymbol{b})$ and receives from node $(\boldsymbol{c})$ (*e.g.,* user terminals), both operating in HD mode, as shown in Fig. 1. Thus, node k is equipped with $N_{t,k}$ antenna elements

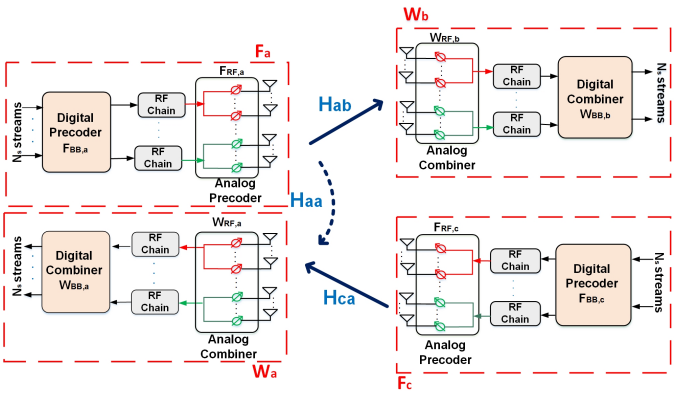

Fig. 1: A mmWave MIMO network with partially-connected hybrid beamformers and one FD node.

and $L_{t,k}$ RF chains to transmit $N_{s,k}$ data streams to node u, equipped with $N_{r,u}$ antennas and $L_{r,u}$ RF chains, where $(k,u) \in \{(c,a),(a,b)\}$. It is assumed that the HD nodes are sufficiently away from each other, so that transmission from node $(\boldsymbol{c})$ does not interfere node $(\boldsymbol{b})$.

The hybrid precoder $\boldsymbol{F}_k = \boldsymbol{F}_{\mathrm{RF},k}\boldsymbol{F}_{\mathrm{BB},k} \in \mathbb{C}^{N_{t,k}\times N_{s,k}}$ consists of a baseband precoder $\boldsymbol{F}_{\mathrm{BB},k} \in \mathbb{C}^{N_{t,k}\times L_{t,k}}$, and an analog RF precoder $\boldsymbol{F}_{\mathrm{RF},k} \in \mathbb{C}^{L_{t,k}\times N_{s,k}}$. The transmitted signal can be written as $\boldsymbol{x}_k = \boldsymbol{F}_{\mathrm{RF},k}\boldsymbol{F}_{\mathrm{BB},k}\boldsymbol{s}_k$, where $\boldsymbol{s}_k \in \mathbb{C}^{N_{s,k}}$ is the symbol vector, with zero mean and covariance $\frac{1}{N_{s,k}}\boldsymbol{I}_{N_{s,k}}$. The transmit power is constrained by imposing $\|\boldsymbol{F}_{\mathrm{RF},k}\boldsymbol{F}_{\mathrm{BB},k}\|_F^2 = N_{s,k}$.

The channel matrix from node k to node u is denoted $\boldsymbol{H}_{ku} \in \mathbb{C}^{N_{r,u}\times N_{t,k}}$, assumed normalized so that $\|\boldsymbol{H}_{ku}\|_F^2 = N_{t,k}N_{r,u}$. For the intended links ($\boldsymbol{H}_{ca}$ and $\boldsymbol{H}_{ab}$), we assume a narrowband clustered channel based on the Saleh-Valenzuela model [13], which can be represented as

$$\boldsymbol{H} = \sum_{n=1}^{N_{cl}}\sum_{m=1}^{N_{ray}} \alpha_{m,n}\boldsymbol{a}_{\mathrm{R}}\left(\phi^{m,n}\right)\boldsymbol{a}_{\mathrm{T}}^H\left(\theta^{m,n}\right) \tag{1}$$

where $\alpha_{m,n}$, $\phi^{m,n}$ and $\theta^{m,n}$ respectively denote the complex gain, angle of arrival (AoA) and of departure (AoD) of the (m,n) path, and $\boldsymbol{a}_{\mathrm{T}}(\theta)$, $\boldsymbol{a}_{\mathrm{R}}(\phi)$ denote the transmit and receive array steering vectors. N_{cl} and N_{ray} represent the total number of clusters and rays per cluster, respectively. The SI channel $\boldsymbol{H}_{aa} \in \mathbb{C}^{N_{r,a}\times N_{t,a}}$ consists of a near-field line-of-sight (LOS) component and a far-field component due to non-line-of-sight (NLOS) reflections:

$$\boldsymbol{H}_{aa} = \sqrt{\frac{\kappa}{\kappa+1}}\boldsymbol{H}_{aa}^{\mathrm{LOS}} + \sqrt{\frac{1}{\kappa+1}}\boldsymbol{H}_{aa}^{\mathrm{NLOS}}, \tag{2}$$

where κ is the Rice factor. $\boldsymbol{H}_{aa}^{\mathrm{NLOS}}$ is assumed to follow (1), whereas a near-field model [7] is adopted for the LOS component. Its (p,q) element is $\boldsymbol{H}_{aa}^{\mathrm{LOS}}(p,q) = \frac{\gamma}{r_{pq}}\exp\left(-j\frac{2\pi}{\lambda}r_{pq}\right)$, where γ is a normalization constant, λ is the wavelength, and r_{pq} is the distance between the n-th transmit and m-th receive antennas of node $(\boldsymbol{a})$.

At the receiver of the $k \to u$ link, a hybrid combiner $\boldsymbol{W}_u = \boldsymbol{W}_{\mathrm{RF},u}\boldsymbol{W}_{\mathrm{BB},u}$ is employed, consisting of an analog RF combiner $\boldsymbol{W}_{\mathrm{RF},u} \in \mathbb{C}^{N_{r,u}\times L_{r,u}}$ and a digital baseband combiner $\boldsymbol{W}_{\mathrm{BB},u} \in \mathbb{C}^{L_{r,u}\times N_{s,k}}$.

The PC structure is assumed for the analog RF precoders and combiners. Thus, each transmit (resp. receive) RF chain is connected to $T_{t,k} = N_{t,k}/L_{t,k}$ (resp. $T_{r,u} = N_{r,u}/L_{r,u}$) antennas[1], so that $\boldsymbol{F}_{\mathrm{RF},k}$ and $\boldsymbol{W}_{\mathrm{RF},u}$ are block-diagonal:

$$\boldsymbol{F}_{\mathrm{RF},k} = \mathrm{blkdiag}\left(\boldsymbol{f}_{k,1},\, \boldsymbol{f}_{k,2},\, \cdots,\, \boldsymbol{f}_{k,L_{t,k}}\right), \tag{3}$$

$$\boldsymbol{W}_{\mathrm{RF},u} = \mathrm{blkdiag}\left(\boldsymbol{w}_{u,1},\, \boldsymbol{w}_{u,2},\, \cdots,\, \boldsymbol{w}_{u,L_{r,u}}\right), \tag{4}$$

with $\boldsymbol{f}_{k,v} \in \mathbb{V}_B^{T_{t,k}}$, $\boldsymbol{w}_{u,v} \in \mathbb{V}_B^{T_{r,u}}$ the vectors of complex gains for the v-th RF chain. Analog beamforming is implemented with B-bit resolution phase shifters, and thus $\mathbb{V}_B^T \subset \mathbb{C}^T$ denotes the set of unit-norm vectors whose entries have magnitude $\frac{1}{\sqrt{T}}$ and phase values in $\left\{2\pi\ell/2^B,\, \ell = 0,1,\ldots,2^B-1\right\}$. Note that, in this way, $\boldsymbol{F}_{\mathrm{RF},k}$ and $\boldsymbol{W}_{\mathrm{RF},u}$ are semi-unitary.

The post-combining vector at node $(\boldsymbol{a})$ is presented as

$$\boldsymbol{y}_a = \underbrace{\sqrt{\rho_c}\boldsymbol{W}_a^H\boldsymbol{H}_{ca}\boldsymbol{F}_c\boldsymbol{s}_c}_{\text{desired signal}} + \underbrace{\sqrt{\eta_a}\boldsymbol{W}_a^H\boldsymbol{H}_{aa}\boldsymbol{F}_a\boldsymbol{z}_a + \boldsymbol{W}_a^H\boldsymbol{n}_a}_{\text{SI + noise}} \tag{5}$$

with ρ_c the power gain of the $\boldsymbol{c} \to \boldsymbol{a}$ link, η_a the power gain of the SI channel, $\boldsymbol{n}_a \sim \mathcal{CN}\left(0, \sigma_a^2\boldsymbol{I}_{N_{r,a}}\right)$ the white Gaussian noise at node $(\boldsymbol{a})$, and $\boldsymbol{z}_a$ the SI component, assumed zero-mean with covariance $\frac{1}{N_{s,a}}\boldsymbol{I}_{N_{s,a}}$. Note that, in general, $\boldsymbol{z}_a$ need not be equal to $\boldsymbol{s}_a$, due to delay and distortion introduced by imperfections in the analog front-ends. Letting $\epsilon_{ca} = \frac{\rho_c}{\sigma_a^2}$ and $\epsilon_{aa} = \frac{\eta_a}{\sigma_a^2}$ be the SNR and INR at the receiver of node $(\boldsymbol{a})$, respectively, and assuming Gaussianity of data and SI, the SE of the $\boldsymbol{c} \to \boldsymbol{a}$ link is given by

$$\mathcal{R}_{ca} = \log_2\left|\boldsymbol{I}_{N_s} + \frac{\epsilon_{ca}}{N_{s,c}}\bar{\boldsymbol{H}}_{ca}^H\boldsymbol{R}_a^{-1}\bar{\boldsymbol{H}}_{ca}\right|, \tag{6}$$

where $\bar{\boldsymbol{H}}_{ca} = \boldsymbol{W}_a^H\boldsymbol{H}_{ca}\boldsymbol{F}_c$ is the effective $\boldsymbol{c} \to \boldsymbol{a}$ channel, and $\boldsymbol{R}_a = \frac{\epsilon_{aa}}{N_{s,a}}\boldsymbol{W}_a^H\boldsymbol{H}_{aa}\boldsymbol{F}_a\boldsymbol{F}_a^H\boldsymbol{H}_{aa}^H\boldsymbol{W}_a + \boldsymbol{W}_a^H\boldsymbol{W}_a$, so that $\sigma_a^2\boldsymbol{R}_a$ is the SI + noise covariance matrix at node $(\boldsymbol{a})$. On the other hand, the post-combining vector at node $(\boldsymbol{b})$ is

$$\boldsymbol{y}_b = \sqrt{\rho_a}\boldsymbol{W}_b^H\boldsymbol{H}_{ab}\boldsymbol{F}_a\boldsymbol{s}_a + \boldsymbol{W}_b^H\boldsymbol{n}_b \tag{7}$$

where $\boldsymbol{n}_b \sim \mathcal{CN}\left(0, \sigma_b^2\boldsymbol{I}_{N_{r,b}}\right)$. The SE of the $\boldsymbol{a} \to \boldsymbol{b}$ link is

$$\mathcal{R}_{ab} = \log_2\left|\boldsymbol{I}_{N_s} + \frac{\epsilon_{ab}}{N_{s,a}}\bar{\boldsymbol{H}}_{ab}^H\boldsymbol{R}_b^{-1}\bar{\boldsymbol{H}}_{ab}\right| \tag{8}$$

with $\epsilon_{ab} = \frac{\rho_a}{\sigma_b^2}$ the SNR at node $(\boldsymbol{b})$, $\bar{\boldsymbol{H}}_{ab} = \boldsymbol{W}_b^H\boldsymbol{H}_{ab}\boldsymbol{F}_a$ the effective $\boldsymbol{a} \to \boldsymbol{b}$ channel, and $\boldsymbol{R}_b = \boldsymbol{W}_b^H\boldsymbol{W}_b$. Ideally, we would like to maximize the achievable sum rate, which translates into the following optimization problem:

$$\max_{\mathcal{A}} \quad \mathcal{R}_{ca} + \mathcal{R}_{ab} \tag{9a}$$

$$\text{s.t.} \quad \|\boldsymbol{F}_{\mathrm{RF},a}\boldsymbol{F}_{\mathrm{BB},a}\|_F^2 = N_{s,a},\ \|\boldsymbol{F}_{\mathrm{RF},c}\boldsymbol{F}_{\mathrm{BB},c}\|_F^2 = N_{s,c}, \tag{9b}$$

$$\boldsymbol{F}_{\mathrm{RF},a} = \mathrm{blkdiag}\left(\boldsymbol{f}_{a,1},...,\boldsymbol{f}_{a,L_{t,a}}\right), \quad \boldsymbol{f}_{a,v} \in \mathbb{V}_B^{T_{t,a}} \tag{9c}$$

$$\boldsymbol{F}_{\mathrm{RF},c} = \mathrm{blkdiag}\left(\boldsymbol{f}_{c,1},...,\boldsymbol{f}_{c,L_{t,c}}\right), \quad \boldsymbol{f}_{c,v} \in \mathbb{V}_B^{T_{t,c}} \tag{9d}$$

$$\boldsymbol{W}_{\mathrm{RF},a} = \mathrm{blkdiag}\left(\boldsymbol{w}_{a,1},...,\boldsymbol{w}_{a,L_{r,a}}\right), \quad \boldsymbol{w}_{a,v} \in \mathbb{V}_B^{T_{r,a}} \tag{9e}$$

$$\boldsymbol{W}_{\mathrm{RF},b} = \mathrm{blkdiag}\left(\boldsymbol{w}_{b,1},...,\boldsymbol{w}_{b,L_{r,b}}\right), \quad \boldsymbol{w}_{b,v} \in \mathbb{V}_B^{T_{r,b}} \tag{9f}$$

[1]For simplicity, we assume $T_{t,k}$, $T_{r,u}$ are integers.

where $\mathcal{A} = \{\boldsymbol{F}_{\mathrm{RF},c}, \boldsymbol{F}_{\mathrm{BB},c}, \boldsymbol{F}_{\mathrm{RF},a}, \boldsymbol{F}_{\mathrm{BB},a}, \boldsymbol{W}_{\mathrm{RF},a}, \boldsymbol{W}_{\mathrm{BB},a}, \boldsymbol{W}_{\mathrm{RF},b}, \boldsymbol{W}_{\mathrm{BB},b}\}$. The transmit power constraints at nodes ($\boldsymbol{a}$) and ($\boldsymbol{c}$) are reflected in (9b), whereas (9c)-(9f) capture the hardware-related constraints imposed by the PC structure.

III. Hybrid Beamforming Design

Since (9) is highly nonconvex, we shall decouple the designs of the analog and digital stages. First, let us define

$$\widetilde{\boldsymbol{z}}_a = \boldsymbol{F}_{\mathrm{BB},a}\boldsymbol{z}_a \in \mathbb{C}^{L_{t,a}}, \quad \widetilde{\boldsymbol{s}}_k = \boldsymbol{F}_{\mathrm{BB},k}\boldsymbol{s}_k \in \mathbb{C}^{L_{t,k}}, \tag{10}$$

for $k \in \{a, c\}$. Note that under the power constraints (9b), and since the RF precoders are semi-unitary, it follows that $\|\boldsymbol{F}_{\mathrm{BB},k}\|_F^2 = N_{s,k}$, and therefore

$$E\{\|\widetilde{\boldsymbol{z}}_a\|^2\} = 1, \quad E\{\|\widetilde{\boldsymbol{s}}_k\|^2\} = 1, \ k \in \{a, c\}. \tag{11}$$

A. Analog RF Beamforming

Consider the outputs of RF combiners at nodes ($\boldsymbol{a}$) and ($\boldsymbol{b}$):

$$\begin{aligned}\widetilde{\boldsymbol{y}}_a &= \sqrt{\rho}_c \boldsymbol{W}_{\mathrm{RF},a}^H \boldsymbol{H}_{ca}\boldsymbol{F}_{\mathrm{RF},c}\widetilde{\boldsymbol{s}}_c + \boldsymbol{W}_{\mathrm{RF},a}^H \boldsymbol{n}_a \\ &\quad + \sqrt{\eta_a}\boldsymbol{W}_{\mathrm{RF},a}^H \boldsymbol{H}_{aa}\boldsymbol{F}_{\mathrm{RF},a}\widetilde{\boldsymbol{z}}_a, \qquad (12)\\ \widetilde{\boldsymbol{y}}_b &= \sqrt{\rho}_a \boldsymbol{W}_{\mathrm{RF},b}^H \boldsymbol{H}_{ab}\boldsymbol{F}_{\mathrm{RF},a}\widetilde{\boldsymbol{s}}_a + \boldsymbol{W}_{\mathrm{RF},b}^H \boldsymbol{n}_b. \qquad (13)\end{aligned}$$

Note, $\widetilde{\boldsymbol{y}}_a \in \mathbb{C}^{L_{r,a}}$, $\widetilde{\boldsymbol{y}}_b \in \mathbb{C}^{L_{r,b}}$ depend on the as-yet-unknown baseband precoders. To sidestep this issue we adopt the following assumption, consistent with (11), about the covariance matrices of the vectors in (10):

$$E\left\{\widetilde{\boldsymbol{z}}_a\widetilde{\boldsymbol{z}}_a^H\right\} \approx \tfrac{1}{L_{t,a}}\boldsymbol{I}_{L_{t,a}}, \qquad E\left\{\widetilde{\boldsymbol{s}}_k\widetilde{\boldsymbol{s}}_k^H\right\} \approx \tfrac{1}{L_{t,k}}\boldsymbol{I}_{L_{t,k}}. \tag{14}$$

With this, from (12)-(13) the signal-to-SI-plus-noise ratio (SSINR) at the output of the analog combiner at ($\boldsymbol{a}$), as well as the SNR at the output of the analog combiner at ($\boldsymbol{b}$), will not depend on baseband precoders, and respectively become

$$\mathrm{SSINR}_{ca} = \frac{\frac{\epsilon_{ca}}{L_{t,c}}\|\boldsymbol{W}_{\mathrm{RF},a}^H \boldsymbol{H}_{ca}\boldsymbol{F}_{\mathrm{RF},c}\|_F^2}{\frac{\epsilon_{aa}}{L_{t,a}}\|\boldsymbol{W}_{\mathrm{RF},a}^H \boldsymbol{H}_{aa}\boldsymbol{F}_{\mathrm{RF},a}\|_F^2 + \|\boldsymbol{W}_{\mathrm{RF},a}^H\|_F^2}, \tag{15}$$

$$\mathrm{SNR}_{ab} = \frac{\frac{\epsilon_{ab}}{L_{t,a}}\|\boldsymbol{W}_{\mathrm{RF},b}^H \boldsymbol{H}_{ab}\boldsymbol{F}_{\mathrm{RF},a}\|_F^2}{\|\boldsymbol{W}_{\mathrm{RF},b}^H\|_F^2}. \tag{16}$$

Note, (15)-(16) are coupled by $\boldsymbol{F}_{\mathrm{RF},a}$. Both $\boldsymbol{F}_{\mathrm{RF},a}$ and $\boldsymbol{W}_{\mathrm{RF},a}$ must strike a balance between SI suppression and beamforming to the intended channels $\boldsymbol{H}_{ab}$ and $\boldsymbol{H}_{ca}$ resp. To this end, it makes sense to maximize some (increasing) function of (15)-(16). We propose to take the *product* of these two quantities as objective, as it will be conducive to its maximization:

$$\max_{\boldsymbol{F}_{\mathrm{RF},c},\boldsymbol{F}_{\mathrm{RF},a},\boldsymbol{W}_{\mathrm{RF},a},\boldsymbol{W}_{\mathrm{RF},b}} \mathrm{SSINR}_{ca}\cdot\mathrm{SNR}_{ab} \quad \text{s.t.} \quad (9c),(9d),(9e),(9f) \tag{17}$$

To tackle (17) under the hardware-related constraints, we adopt a cyclic approach by sequentially optimizing with respect to each term while keeping the others fixed, and then iterate. In this way, the following four subproblems are obtained:

- Given $\boldsymbol{W}_{\mathrm{RF},a}$, let $\boldsymbol{G} = \boldsymbol{H}_{ca}^H \boldsymbol{W}_{\mathrm{RF},a}\boldsymbol{W}_{\mathrm{RF},a}^H \boldsymbol{H}_{ca}$ and solve

$$\max_{\boldsymbol{F}_{\mathrm{RF},c}} \mathsf{Tr}\left(\boldsymbol{F}_{\mathrm{RF},c}^H \boldsymbol{G}\boldsymbol{F}_{\mathrm{RF},c}\right) \quad \text{s.t} \quad (9d) \tag{18}$$

- Given $\boldsymbol{F}_{\mathrm{RF},a}$, let $\boldsymbol{G} = \boldsymbol{H}_{ab}\boldsymbol{F}_{\mathrm{RF},a}\boldsymbol{F}_{\mathrm{RF},a}^H \boldsymbol{H}_{ab}^H$ and solve

$$\max_{\boldsymbol{W}_{\mathrm{RF},b}} \mathsf{Tr}\left(\boldsymbol{W}_{\mathrm{RF},b}^H \boldsymbol{G}\boldsymbol{W}_{\mathrm{RF},b}\right) \quad \text{s.t.} \quad (9f) \tag{19}$$

- Given $\boldsymbol{W}_{\mathrm{RF},b}, \boldsymbol{W}_{\mathrm{RF},a}$, let $\boldsymbol{A} = \boldsymbol{H}_{ab}^H \boldsymbol{W}_{\mathrm{RF},b}\boldsymbol{W}_{\mathrm{RF},b}^H \boldsymbol{H}_{ab}$, $\boldsymbol{B} = \boldsymbol{H}_{aa}^H \boldsymbol{W}_{\mathrm{RF},a}\boldsymbol{W}_{\mathrm{RF},a}^H \boldsymbol{H}_{aa} + \frac{L_{r,a}}{\epsilon_{aa}}\boldsymbol{I}_{N_{r,a}}$, and solve

$$\max_{\boldsymbol{F}_{\mathrm{RF},a}} \frac{\mathsf{Tr}\left(\boldsymbol{F}_{\mathrm{RF},a}^H \boldsymbol{A}\boldsymbol{F}_{\mathrm{RF},a}\right)}{\mathsf{Tr}\left(\boldsymbol{F}_{\mathrm{RF},a}^H \boldsymbol{B}\boldsymbol{F}_{\mathrm{RF},a}\right)} \quad \text{s.t.} \quad (9c) \tag{20}$$

- Given $\boldsymbol{F}_{\mathrm{RF},c}, \boldsymbol{F}_{\mathrm{RF},a}$, let $\boldsymbol{A} = \boldsymbol{H}_{ac}\boldsymbol{F}_{\mathrm{RF},c}\boldsymbol{F}_{\mathrm{RF},c}^H \boldsymbol{H}_{ac}^H$, $\boldsymbol{B} = \boldsymbol{H}_{aa}\boldsymbol{F}_{\mathrm{RF},a}\boldsymbol{F}_{\mathrm{RF},a}^H \boldsymbol{H}_{aa}^H + \frac{L_{r,a}}{\epsilon_{aa}}\boldsymbol{I}_{N_{r,a}}$, and solve

$$\max_{\boldsymbol{W}_{\mathrm{RF},a}} \frac{\mathsf{Tr}\left(\boldsymbol{W}_{\mathrm{RF},a}^H \boldsymbol{A}\boldsymbol{W}_{\mathrm{RF},a}\right)}{\mathsf{Tr}\left(\boldsymbol{W}_{\mathrm{RF},a}^H \boldsymbol{B}\boldsymbol{W}_{\mathrm{RF},a}\right)} \quad \text{s.t} \quad (9e) \tag{21}$$

1) Analog beamformers at HD nodes: Problems (18)-(19) are instances of the following generic problem:

$$\max_{\boldsymbol{X}} \quad \mathsf{Tr}\left(\boldsymbol{X}^H \boldsymbol{G}\boldsymbol{X}\right) \tag{22}$$

$$\text{s.t.} \quad \boldsymbol{X} = \mathrm{blkdiag}\left(\boldsymbol{x}_1, \cdots, \boldsymbol{x}_L\right), \quad \boldsymbol{x}_v \in \mathbb{V}_B^T \ \forall v \tag{23}$$

where $\boldsymbol{G} \in \mathbb{C}^{M\times M}$ is Hermitian positive semidefinite, and M, L, T respectively represent the number of antennas, RF chains, and the number of antennas connected to each RF chain. Let $\overline{\boldsymbol{x}}_v$ be the v-th column of $\boldsymbol{X}$, and let $\overline{\boldsymbol{X}}_v \in \mathbb{C}^{M\times(L-1)}$ be the matrix obtained by deleting $\overline{\boldsymbol{x}}_v$ from $\boldsymbol{X}$. Then $\mathsf{Tr}\left(\boldsymbol{X}^H\boldsymbol{G}\boldsymbol{X}\right) = \overline{\boldsymbol{x}}_v^H\boldsymbol{G}\overline{\boldsymbol{x}}_v + \mathsf{Tr}\left(\overline{\boldsymbol{X}}_v^H\boldsymbol{G}\overline{\boldsymbol{X}}_v\right)$. Noting that $\overline{\boldsymbol{x}}_v$ has only T nonzero entries, comprised in $\boldsymbol{x}_v$, let us define $\overline{\boldsymbol{G}}_v \in \mathbb{C}^{T\times T}$ as the submatrix of $\boldsymbol{G}$ corresponding to rows and columns $(v-1)T+1$ through vT. Then $\overline{\boldsymbol{x}}_v^H\boldsymbol{G}\overline{\boldsymbol{x}}_v = \boldsymbol{x}_v^H\overline{\boldsymbol{G}}_v\boldsymbol{x}_v$, and the problem boils down to

$$\max_{\boldsymbol{x}_v} \ \boldsymbol{x}_v^H\overline{\boldsymbol{G}}_v\boldsymbol{x}_v \quad \text{s.t.} \quad \boldsymbol{x}_v \in \mathbb{V}_B^T, \tag{24}$$

which can be approximately solved by sequentially optimizing each entry of $\boldsymbol{x}_v$ assuming all others fixed, and iterating until convergence. For details, please refer to [9, App. C].

2) Analog beamformers at FD node: Problems (20)-(21) are instances of the following generic problem:

$$\max_{\boldsymbol{X}} \frac{\mathsf{Tr}\left(\boldsymbol{X}^H\boldsymbol{A}\boldsymbol{X}\right)}{\mathsf{Tr}\left(\boldsymbol{X}^H\boldsymbol{B}\boldsymbol{X}\right)} \quad \text{s.t.} \quad (23) \tag{25}$$

where $\boldsymbol{A}, \boldsymbol{B} \in \mathbb{C}^{M\times M}$ are Hermitian positive semidefinite, and $\boldsymbol{X} \in \mathbb{C}^{M\times L}$. The hardware-related constraints (23) make (25) hard to solve exactly, so we resort again to cyclic entry-by-entry optimization. Focusing on the v-th column of $\boldsymbol{X}$, while keeping the remaining ones fixed, (25) becomes

$$\max_{\boldsymbol{x}_v} \quad \frac{\boldsymbol{x}_v^H\overline{\boldsymbol{A}}_v\boldsymbol{x}_v + \widetilde{a}_v}{\boldsymbol{x}_v^H\overline{\boldsymbol{B}}_v\boldsymbol{x}_v + \widetilde{b}_v} \quad \text{s.t.} \quad \boldsymbol{x}_v \in \mathbb{V}_B^T \tag{26}$$

where $\widetilde{a}_v = \mathsf{Tr}\left(\overline{\boldsymbol{X}}_v^H\boldsymbol{A}\overline{\boldsymbol{X}}_v\right)$, $\widetilde{b}_v = \mathsf{Tr}\left(\overline{\boldsymbol{X}}_v^H\boldsymbol{B}\overline{\boldsymbol{X}}_v\right)$, and $\overline{\boldsymbol{A}}_v$, $\overline{\boldsymbol{B}}_v \in \mathbb{C}^{T\times T}$ are the corresponding submatrices of $\boldsymbol{A}$ and $\boldsymbol{B}$. Now, we can expand the numerator and the denominator in (26) with respect to the n-th entry of $\boldsymbol{x}_v$, say x_{nv}, as follows:

$$\begin{aligned}\boldsymbol{x}_v^H\overline{\boldsymbol{A}}_v\boldsymbol{x}_v + \widetilde{a}_v &= g_{nv} + 2\mathsf{Re}\left\{x_{nv}^*\alpha_{nv}\right\}\\ \boldsymbol{x}_v^H\overline{\boldsymbol{B}}_v\boldsymbol{x}_v + \widetilde{b}_v &= h_{nv} + 2\mathsf{Re}\left\{x_{nv}^*\beta_{nv}\right\}\end{aligned}$$

with $\alpha_{nv} = \sum_{m\neq n} x_{mv}[\overline{\boldsymbol{A}}_v]_{nm}$, $\beta_{nv} = \sum_{m\neq n} x_{mv}[\overline{\boldsymbol{B}}_v]_{nm}$, and, noting that $|x_{nv}| = \frac{1}{\sqrt{T}}$,

$$g_{nv} = \widetilde{a}_v + \frac{1}{T}[\overline{\boldsymbol{A}}_v]_{nn} + \sum_{m\neq n}\sum_{l\neq n} x_{lv}^* x_{mv}[\overline{\boldsymbol{A}}_v]_{lm}, \quad (27)$$

$$h_{nv} = \widetilde{b}_v + \frac{1}{T}[\overline{\boldsymbol{B}}_v]_{nn} + \sum_{m\neq n}\sum_{l\neq n} x_{lv}^* x_{mv}[\overline{\boldsymbol{B}}_v]_{lm}, \quad (28)$$

which are independent of the phase of x_{nv}. We invoke now the following result, adapted from [14, Sec. V-B]:

Lemma 1. *For g, $h \in \mathbb{R}$ and α, $\beta \in \mathbb{C}$, let*

$$f(\theta) = \frac{n(\theta)}{d(\theta)} = \frac{g + 2\mathsf{Re}\left\{\frac{1}{\sqrt{T}} e^{-j\theta}\alpha\right\}}{h + 2\mathsf{Re}\left\{\frac{1}{\sqrt{T}} e^{-j\theta}\beta\right\}}. \quad (29)$$

Assume $g > \frac{2|\alpha|}{\sqrt{T}}$, $h > \frac{2|\beta|}{\sqrt{T}}$, so that $n(\theta) > 0$, $d(\theta) > 0$ for all θ. Then, f attains its maximum at $\boldsymbol{\theta}_{\max} = \angle z + \arcsin\frac{c}{|z|}$, where $z = h\alpha - g\beta$ and $c = \frac{2}{\sqrt{T}}\mathsf{Im}\{\alpha\beta^*\}$.

Thus, Lemma 1 can be used to find a candidate phase θ_{nv}. Then $x_{nv} = \frac{1}{\sqrt{T}} e^{j\mathcal{Q}(\theta_{nv}, B)}$, where $\mathcal{Q}(\cdot, B)$ denotes the phase quantization operation with *B* bits. This process is iterated over all $v \in \{1, \ldots, L\}$ and $n \in \{1, \ldots, T\}$ until convergence.

B. Digital Baseband Beamforming

Once the RF factors of the beamformers have been found, the effective channels $\widetilde{\boldsymbol{H}}_{ca} = \boldsymbol{W}_{\mathrm{RF},a}^H \boldsymbol{H}_{ca} \boldsymbol{F}_{\mathrm{RF},c}$, $\widetilde{\boldsymbol{H}}_{ab} = \boldsymbol{W}_{\mathrm{RF},b}^H \boldsymbol{H}_{ab} \boldsymbol{F}_{\mathrm{RF},a}$ and $\widetilde{\boldsymbol{H}}_{aa} = \boldsymbol{W}_{\mathrm{RF},a}^H \boldsymbol{H}_{aa} \boldsymbol{F}_{\mathrm{RF},a}$ are available, and analogously to (15)-(16) one finds that the SSINR and SNR at the output of the baseband combiners are given by

$$\mathrm{SSINR}'_{ca} = \frac{\frac{\epsilon_{ca}}{N_{s,c}} \|\boldsymbol{W}_{\mathrm{BB},a}^H \widetilde{\boldsymbol{H}}_{ca} \boldsymbol{F}_{\mathrm{BB},c}\|_F^2}{\frac{\epsilon_{aa}}{N_{s,a}} \|\boldsymbol{W}_{\mathrm{BB},a}^H \widetilde{\boldsymbol{H}}_{aa} \boldsymbol{F}_{\mathrm{BB},a}\|_F^2 + \|\boldsymbol{W}_{\mathrm{BB},a}^H\|_F^2}, \quad (30)$$

$$\mathrm{SNR}'_{ab} = \frac{\frac{\epsilon_{ab}}{N_{s,a}} \|\boldsymbol{W}_{\mathrm{BB},b}^H \widetilde{\boldsymbol{H}}_{ab} \boldsymbol{F}_{\mathrm{BB},a}\|_F^2}{\|\boldsymbol{W}_{\mathrm{BB},b}^H\|_F^2}. \quad (31)$$

Thus, we seek to maximize the product of (30) and (31):

$$\max_{\boldsymbol{F}_{\mathrm{BB},c}, \boldsymbol{F}_{\mathrm{BB},a}, \boldsymbol{W}_{\mathrm{BB},a}, \boldsymbol{W}_{\mathrm{BB},b}} \mathrm{SSINR}'_{ca} \cdot \mathrm{SNR}'_{ab} \quad (32)$$
$$\text{s.t.} \quad \boldsymbol{F}_{\mathrm{BB},c}, \boldsymbol{F}_{\mathrm{BB},a}, \boldsymbol{W}_{\mathrm{BB},a}, \boldsymbol{W}_{\mathrm{BB},b} \quad \text{semi-unitary.}$$

We impose a semi-unitary constraint on combiners since the sum rate (9a) is unaffected by this choice. The same constraint is imposed on the precoders for simplicity (thus, the power allocation across streams is uniform, and not optimized). Analogously to the design of the RF factors, we approach (32) by iteratively optimizing one of the four variables while fixing the other three. At each iteration, on one hand $\boldsymbol{F}_{\mathrm{BB},c}$ is taken as the dominant right singular vectors of $\boldsymbol{W}_{\mathrm{BB},a}^H \widetilde{\boldsymbol{H}}_{ca}$, whereas $\boldsymbol{W}_{\mathrm{BB},b}$ is taken as the dominant left singular vectors of $\widetilde{\boldsymbol{H}}_{ab} \boldsymbol{F}_{\mathrm{BB},a}$. On the other hand, for the FD node beamformers,

- Given $\boldsymbol{W}_{\mathrm{BB},b}, \boldsymbol{W}_{\mathrm{BB},a}$, let $\boldsymbol{A} = \widetilde{\boldsymbol{H}}_{ab}^H \boldsymbol{W}_{\mathrm{BB},b} \boldsymbol{W}_{\mathrm{BB},b}^H \widetilde{\boldsymbol{H}}_{ab}$, $\boldsymbol{B} = \widetilde{\boldsymbol{H}}_{aa}^H \boldsymbol{W}_{\mathrm{BB},a} \boldsymbol{W}_{\mathrm{BB},a}^H \widetilde{\boldsymbol{H}}_{aa} + \frac{N_{s,a}}{\epsilon_{aa}} \boldsymbol{I}_{L_{r,a}}$, and solve

$$\max_{\boldsymbol{F}_{\mathrm{BB},a}} \frac{\mathsf{Tr}\left(\boldsymbol{F}_{\mathrm{BB},a}^H \boldsymbol{A} \boldsymbol{F}_{\mathrm{BB},a}\right)}{\mathsf{Tr}\left(\boldsymbol{F}_{\mathrm{BB},a}^H \boldsymbol{B} \boldsymbol{F}_{\mathrm{BB},a}\right)} \text{ s.t. } \boldsymbol{F}_{\mathrm{BB},a} \text{ semi-unitary.} \quad (33)$$

- Given $\boldsymbol{F}_{\mathrm{BB},c}, \boldsymbol{F}_{\mathrm{BB},a}$, let $\boldsymbol{A} = \widetilde{\boldsymbol{H}}_{ac} \boldsymbol{F}_{\mathrm{BB},c} \boldsymbol{F}_{\mathrm{BB},c}^H \widetilde{\boldsymbol{H}}_{ac}^H$, $\boldsymbol{B} = \widetilde{\boldsymbol{H}}_{aa} \boldsymbol{F}_{\mathrm{BB},a} \boldsymbol{F}_{\mathrm{BB},a}^H \widetilde{\boldsymbol{H}}_{aa}^H + \frac{N_{s,a}}{\epsilon_{aa}} \boldsymbol{I}_{N_{s,a}}$, and solve

$$\max_{\boldsymbol{W}_{\mathrm{BB},a}} \frac{\mathsf{Tr}\left(\boldsymbol{W}_{\mathrm{BB},a}^H \boldsymbol{A} \boldsymbol{W}_{\mathrm{BB},a}\right)}{\mathsf{Tr}\left(\boldsymbol{W}_{\mathrm{BB},a}^H \boldsymbol{B} \boldsymbol{W}_{\mathrm{BB},a}\right)} \text{ s.t. } \boldsymbol{W}_{\mathrm{BB},a} \text{ semi-unitary.} \quad (34)$$

Both (33)-(34) are *trace ratio* problems, which can be solved by any of the approaches from [15].

IV. Simulation Results

Consider the setting of Fig. 1, with 50-GHz carrier frequency. The FD node ($\boldsymbol{a}$) is equipped with 32-element arrays, whereas the arrays at the HD nodes ($\boldsymbol{b}, \boldsymbol{c}$) have 16 elements. Half-wavelength uniform linear arrays (ULA) are assumed. The relative geometry of the TX and RX arrays at node ($\boldsymbol{a}$) is as in [9, Fig. 2], with parameters $\delta = 2\lambda$, $\alpha = 0$ and $\beta = \frac{\pi}{2}$. We set $N_{cl} = 6$ and $N_{ray} = 5$ in (1), and $\kappa = 10$ dB in (2). The AoAs/AoDs follow a Gaussian distribution with mean angles uniformly distributed in $[0, \pi]$ and standard deviation 16°. All channel matrices are normalized so that their squared Frobenius norms equal the number of their entries. The FD node has $L_{t,a} = L_{r,a} = 8$ RF chains, whereas for the HD nodes $L_{t,c} = L_{r,b} = 4$. The number of data streams is $N_{s,a} = N_{s,c} = 2$, and the INR at node ($\boldsymbol{a}$) is $\epsilon_{aa} = 20$ dB. Monte Carlo simulations were performed on 200 channel realizations. We consider the following benchmark designs:

- **HD-AD:** Assumes HD operation, with all-digital beamformers given by the singular vectors of the corresponding channels.
- **FD-AD UB:** Assumes FD operation *in the absence of SI* ($\epsilon_{aa} = 0$). Same all-digital beamformers as **HD-AD.** It constitutes the ultimate performance upper bound.
- **HD-PC:** Assumes HD operation with hybrid beamformers based on the PC structure, designed via the alternating optimization framework from [13, Sec. V].
- **FD-PC UB:** Assumes FD operation without SI. Same PC-based hybrid beamformers as **HD-PC.** It constitutes an upper bound for FD designs based on the PC structure.
- **FD-PC WYGX:** The design of Wang *et al.* from [12], which assumes FD operation with PC-based hybrid beamformers. Phase values are directly quantized to account for finite precision of phase shifters.

A. SE Performance

Fig. 2 shows the sum spectral efficiency $\mathcal{R}_{ca} + \mathcal{R}_{ab}$ as a function of the SNR, assumed to be the same at both receivers: $\epsilon_{ca} = \epsilon_{ab}$. The SNR gap between **FD-AD UB** and **FD-PC UB** is 3 dB (resp. 6 dB) for 4-bit (resp. 1-bit) phase shifters, and is solely due to the hardware-related constraints imposed by the PC-based hybrid architecture. Note that these designs assume

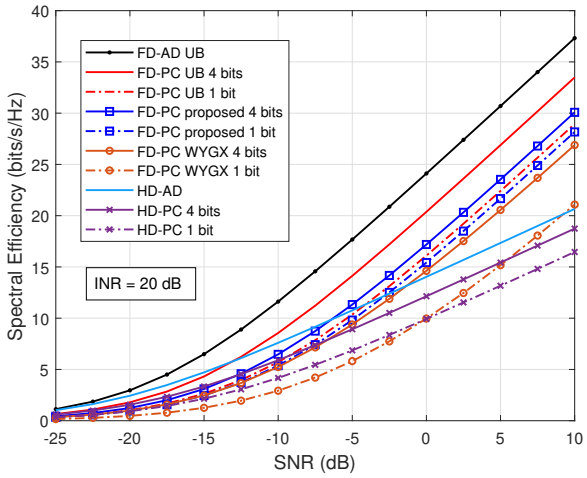

Fig. 2: Spectral Efficiency vs SNR $\epsilon_{ca} = \epsilon_{ab}$.

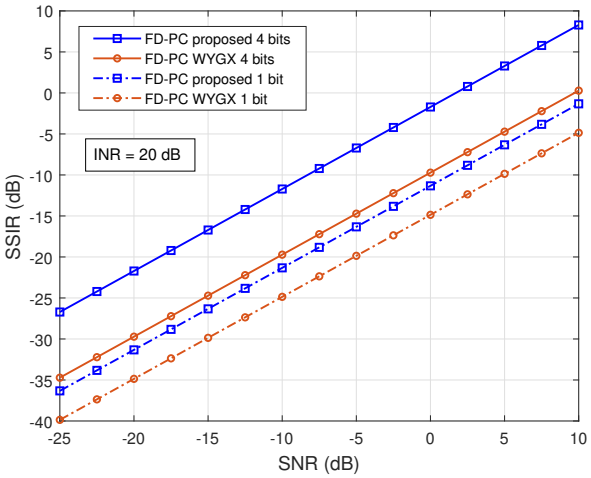

Fig. 3: Worst-case SSIR (averaged over all runs) vs SNR ϵ_{ca}.

no SI, and therefore they are useful only as performance bounds. In practice, SI must be taken into account. In this regard, we can compare our proposed design with that from [12] (**FD-PC WYGX**): we obtain an improvement of 2.7 dB for 4-bit phase shifters, and of 5.5 dB for coarse 1-bit resolution. In fact, the proposed design with 1-bit phase shifters outperforms **FD-PC WYGX** with 4 bits. Note that the loss of our design with respect to **FD-PC UB** is 2.5 dB with 4-bit phase shifters, and only of 0.5 dB with 1 bit.

B. SSIR

To evaluate the effectiveness of the proposed design in mitigating SI at the output of the FD node's RF combiner, we consider the (worst case) *signal-to-self-interference ratio* (SSIR) across receive RF chains, defined as

$$\text{SSIR} = \min_{1\le v\le L_{r,a}} \frac{\frac{\epsilon_{ca}}{N_{s,c}}\left[\boldsymbol{W}_{\text{RF},a}^H \boldsymbol{H}_{ca}\boldsymbol{F}_c\boldsymbol{F}_c^H\boldsymbol{H}_{ca}^H\boldsymbol{W}_{\text{RF},a}\right]_{vv}}{\frac{\epsilon_{aa}}{N_{s,a}}\left[\boldsymbol{W}_{\text{RF},a}^H \boldsymbol{H}_{aa}\boldsymbol{F}_a\boldsymbol{F}_a^H\boldsymbol{H}_{aa}^H\boldsymbol{W}_{\text{RF},a}\right]_{vv}}, \tag{35}$$

which is shown in Fig. 3. With 4-bit phase shifters, the proposed design improves SSIR by about 9 dB with respect to **FD-PC WYGX** from [12], which is significant because in practice the loss of dynamic range at the ADC input may result in further performance losses. With 1-bit phase shifters, an SSIR improvement of 3.5 dB is still achieved.

V. Conclusion

The proposed scheme outperforms previous designs while mitigating SI before A/D conversion, and improves upon HD operation even with coarse phase shifter quantization. Future work should aim at further reducing the gap to the upper bound for the partially-connected structure.

Acknowledgment

Work funded by MCIN/AEI/10.13039/501100011033/ FEDER "A way of making Europe" under project MAYTE (PID2022-136512OB-C22) and fellowship PRE2020-096625 "ESF Investing in your future".

References

[1] W. Chen, X. Lin, J. Lee, A. Toskala, S. Sun, C. F. Chiasserini, and L. Liu, "5G-advanced toward 6G: Past, present, and future," *IEEE J. Sel. Areas Commun.*, vol. 41, no. 6, pp. 1592–1619, 2023.

[2] B. Smida, A. Sabharwal, G. Fodor, G. C. Alexandropoulos, H. A. Suraweera, and C.-B. Chae, "Full-duplex wireless for 6G: Progress brings new opportunities and challenges," *IEEE J. Sel. Areas Commun.*, vol. 41, no. 9, pp. 2729–2750, 2023.

[3] J.-C. Chen, "Hybrid beamforming with discrete phase shifters for millimeter-wave massive MIMO systems," *IEEE Trans. Veh. Technol.*, vol. 66, no. 8, pp. 7604–7608, 2017.

[4] R. W. Heath Jr., N. González-Prelcic, S. Rangan, W. Roh, and A. M. Sayeed, "An overview of signal processing techniques for millimeter wave MIMO systems," *IEEE J. Sel. Topics Signal Process.*, vol. 10, no. 3, pp. 436–453, 2016.

[5] Z. Zhang, K. Long, A. V. Vasilakos, and L. Hanzo, "Full-duplex wireless communications: Challenges, solutions, and future research directions," *Proc. IEEE*, vol. 104, no. 7, pp. 1369–1409, 2016.

[6] M. Mohammadi, Z. Mobini, D. Galappaththige, and C. Tellambura, "A comprehensive survey on full-duplex communication: Current solutions, future trends, and open issues," *IEEE Commun. Surveys Tuts.*, vol. 25, no. 4, pp. 2190–2244, 2023.

[7] Z. Xiao, P. Xia, and X.-G. Xia, "Full-duplex millimeter-wave communication," vol. 24, no. 6, pp. 136–143, 2017.

[8] C. K. Sheemar and D. Slock, "Hybrid beamforming and combining for millimeter wave full duplex massive MIMO interference channel," in *Proc. IEEE Global Commun. Conf. (GLOBECOM)*, 2021, pp. 1–6.

[9] R. López-Valcarce and M. Martínez-Cotelo, "Full-duplex mmwave MIMO with finite-resolution phase shifters," *IEEE Trans. Wireless Commun.*, vol. 21, no. 11, pp. 8979–8994, 2022.

[10] I. P. Roberts, H. B. Jain, S. Vishwanath, and J. G. Andrews, "Millimeter wave analog beamforming codebooks robust to self-interference," in *Proc. IEEE Global Commun. Conf. (GLOBECOM)*, 2021, pp. 1–6.

[11] I. P. Roberts and S. Vishwanath, "Beamforming cancellation design for millimeter-wave full-duplex," in *Proc. IEEE Global Commun. Conf. (GLOBECOM)*, 2019, pp. 1–6.

[12] G. Wang, Z. Yang, T. Gong, and C. Xie, "Self-interference cancellation based hybrid beamforming design for full-duplex mmwave communication with partially-connected structures," in *Proc. IEEE Int. Conf. Commun. Technol.*, 2020, pp. 366–371.

[13] X. Yu, J.-C. Shen, J. Zhang, and K. B. Letaief, "Alternating minimization algorithms for hybrid precoding in millimeter wave MIMO systems," *IEEE J. Sel. Topics Signal Process.*, vol. 10, no. 3, pp. 485–500, 2016.

[14] F. Sohrabi and W. Yu, "Hybrid digital and analog beamforming design for large-scale antenna arrays," *IEEE J. Sel. Topics Signal Process.*, vol. 10, no. 3, pp. 501–513, 2016.

[15] Y. Jia, F. Nie, and C. Zhang, "Trace ratio problem revisited," *IEEE Trans. Neural Netw.*, vol. 20, no. 4, pp. 729–735, 2009.